

# A Two-Port Bilateral Model for Semiconductor Lasers

Arthur James Lowery

**Abstract**—A bilateral two-port model of a semiconductor laser that includes bidirectional electronic and photonic interfaces is developed by combining an equivalent circuit laser model and a transmission-line laser model (TLLM). The new model includes chip and package parasitics, gain nonlinearities, and a detailed optical cavity model based on optical traveling waves. This model can be applied to a variety of device structures to simulate optical spectra, optical and electrical waveforms, intensity spectra, and noise characteristics. Three examples demonstrate the flexibility of the model: 1) transient response simulation of semiconductor lasers, 2) characteristics of lasers used as detectors, and 3) coherence collapse in lasers with optical feedback. In all cases, the results are in good agreement with experimental measurements.

## I. INTRODUCTION

THE ideal semiconductor laser model would mimic the operation of the real device in every detail, simulating all observables of the laser while accounting for all variations in device structure, processing, drive electronics, and external optical components [1]. The model could be connected to other device models to form an optical system model. Such a model would hasten the design of photonic devices, circuits, and systems and could be used for detailed optimization for particular applications.

Unfortunately, limitations in computing resources require that simplifications and assumptions have to be made before a model is developed. Many optoelectronic device models use rate equations to describe the interactions between the average electron and photon populations in the device [1], [2]. Numerous adaptations of this technique have been proposed. For example, using a photon rate equation for each longitudinal laser mode gives the laser's spectrum during modulation [3] and dynamic frequency shifting (chirping) may be estimated from the transient responses of both populations [4]. The laser rate equations may also describe saturation in laser amplifiers [5], the dynamic behavior of mode-locked lasers [6], and the transient response of cleaved-coupled-cavity lasers [7].

One problem with using photon density as a variable is that it does not contain optical phase information. Optical phase is important when there is a set of coupled optical

resonators such as in coupled-cavity lasers, external-cavity lasers, distributed-feedback (DFB) lasers, or even Fabry-Perot lasers with unintentional feedback from external components. In these cases, the output wavelength of the device, and its current to light characteristics, are determined by optical interference between the resonators. Although rate equations can be used in simple cases, by calculating effective reflection coefficients at discrete wavelengths [7], finding these wavelengths becomes difficult with multiple resonators exhibiting gain and variable refractive indices, such as in the DFB laser [8].

A development of the rate-equation approach is to use a SPICE-compatible equivalent circuit of the laser diode. This may be used to find the time-varying photon density for a given drive current waveform or, alternatively, to find the frequency response of the device [9]. This approach has an advantage that it includes parasitic components in the laser chip and mount and can be linked to models of the drive circuit for evaluation of the systems response to modulation.

An alternative variable to photon density is optical field. An optical field contains phase information and thus offers the possibility of dealing with multiple reflections. The optical field within a resonator system may be solved in the frequency domain or in the time domain. Frequency-domain models often use a transfer-matrix description of the laser that may be obtained by multiplying together the transfer matrices describing each individual reflection [10]. Unfortunately, if the spectrum of a modulated laser is required, the multiplication has to be performed for each wavelength at each timestep [8]. This is computationally inefficient.

Time-domain models using optical fields are better suited to modulated devices with multiple resonators than frequency-domain models because the former are simpler to develop and require less computation. Time-domain optical-field models are commonly based on scattering matrix descriptions of the individual reflections and of the gain medium [11 and references therein]. The scattering matrices may be connected by delays (transmission lines) so that reflected waves out of one scattering matrix reach adjacent matrices after the delay. The delays represent the optical propagation time along a portion of the waveguide. Solution of the network is by iteration, each iteration representing an increase in time equal to the delay.

This paper develops a new laser model that combines the best features of two previous modeling techniques for

Manuscript received February 13, 1991; revised June 12, 1991. This work was supported by the Australian Research Council.

The author is with the Photonics Research Laboratory, Department of Electrical and Electronic Engineering, University of Melbourne, Parkville, Victoria 3052, Australia.

IEEE Log Number 9103664.

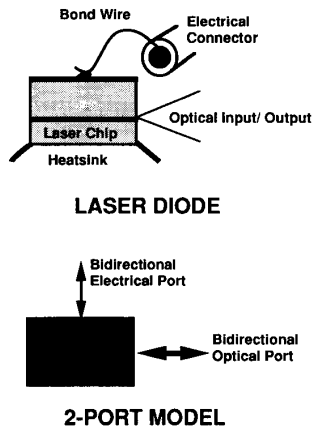


Fig. 1. A semiconductor laser (top) and its two-port model (bottom).

semiconductor lasers: the equivalent circuit model, developed by Tucker and others [9], and a time-domain optical-field model, the transmission-line laser model (TLLM), developed by Lowery [11]–[13]. The new model includes chip-and-package parasitics, multimode operation, complex optical structures, and bidirectional electronic and photonic interfaces, allowing it to be cascaded with other electronic or photonic device models. The model is able to predict results obtained by previous rate-equation models [2]–[7] without having to recompile the computer program. This is an important step toward the development of a universal photonic-CAD package, similar to present electronic and microwave-CAD packages.

Fig. 1 shows a laser device and the proposed model. The model may be thought of as a scattering matrix with memory, which responds to optical and electrical inputs in the time domain and outputs optical and electrical waves. This paper covers the development and testing of the new model. Section II details the modifications required to link the equivalent circuit model and the TLLM. Section III presents results from three applications of the model: 1) simulation of the transient response of a laser, 2) assessment of the performance of laser as an optical detector, and 3) effects of optical feedback on lasers, in particular coherence collapse, intensity noise, and intensity waveform. These applications demonstrate the versatility of the new model. Section IV is the conclusion.

## II. COMBINING THE TWO MODELS

Fig. 2 shows the features of the equivalent circuit model [Fig. 2(a)], the transmission-line laser model [Fig. 2(b)] and the combined model [Fig. 2(c)] schematically. The equivalent circuit model has a bidirectional electronic interface and a unidirectional photonic interface based on photon density [9], [14]. The unidirectional photonic interface cannot accept reflected waves, back into the laser. Also, the photonic interface does not provide any spectral information. The carrier and photon densities in the model are averaged over the entire laser cavity and so the effects of inhomogeneities within a device are ignored.

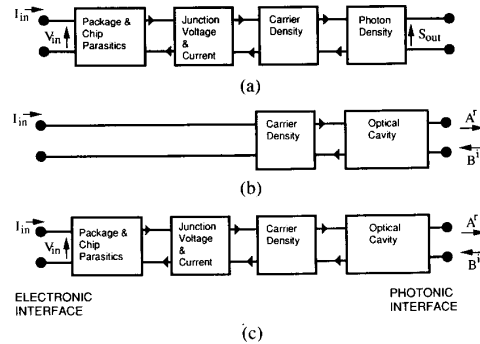


Fig. 2. Schematic representations of (a) Tucker's equivalent circuit model, (b) the transmission-line laser model, and (c) the new combined model.

The transmission-line laser model (TLLM), shown in Fig. 2(b), has a unidirectional electronic interface and a bidirectional photonic interface in terms of optical field [11]. Because the electronic interface is unidirectional, it cannot include any interactions with external components on its electrical port. However, the bidirectional photonic interface allows consideration of external optical components. The use of an optical field, rather than photon density, at the photonic interface enables the phase of reflected waves to be considered and also enables the laser's output spectrum to be calculated using Fourier transforms. The optical cavity model in the TLLM is based on traveling-wave equations for the optical field and the field equations are solved by iteration. This cavity model is very flexible: transmission-line laser models of Fabry-Perot lasers, distributed feedback lasers, external cavity lasers, and laser amplifiers have already been demonstrated [11]. The model includes the effects of carrier and photon inhomogeneities by splitting the cavity longitudinally, into a number of model sections. The gain dynamics are treated by including carrier-density rate equations within each section. A detailed review of the technique may be found in [11].

The combined model [Fig. 2(c)] uses the electrical interface of the equivalent circuit model and the photonic interface of the transmission-line laser model to give a model with bidirectional electrical and photonic interfaces (i.e., a bilateral model). This two-port model can be used for many situations such as laser sources and laser detectors. It can also form part of a system model. The combining of the models is now described in detail.

### A. Bidirectional Electronic Interface and Parasitic Components

Including a bidirectional electrical interface in the model allows the effects of drive circuits to be studied. A bidirectional interface can be provided by calculation of the laser's junction voltage from the carrier density. However, a more complete laser model would include chip parasitics and package parasitics as well as a bidirectional interface. Tucker and Kaminow developed such a model for ridge-waveguide lasers [14], which was solved using

a circuit analysis package, such as SPICE [15]. The TLLM requires a custom-written program based on an iterative scatter-connect algorithm, the basis of all transmission-line models (TLM's) [11]. If parasitic components are to be added to the TLLM, they must be converted to transmission-line equivalents before a scatter-connect algorithm is developed.

Tucker and Kaminow's equivalent circuit model of the device and chip parasitics is given in Fig. 3(a). The components are listed in Table I and their purposes is explained in [14]. A short length of a 50  $\Omega$  transmission line is included to represent the input connector to the laser package. In TLM, inductors and capacitors in the equivalent circuit model may be represented by either link transmission lines or stub transmission lines [16]. The transmission-line representation of the parasitic components is given in Fig. 3(b). The model calculates the voltage across the input port and the injection current into the active region of the laser from the input current into the laser package and the carrier density in the active region.

The model is divided into four scattering zones, each with a single circuit node. The circuit nodes are labeled  $e, f, g, h$ . The scattering nodes are connected with link-transmission lines with a delay of one iteration timestep. This delay allows an explicit algorithm to be generated; each scattering event uses data from the previous iteration. Without the delays, the scattering events in every node would have to be solved simultaneously [16].

The link transmission-lines also serve to represent three of the reactive components. The link line between nodes  $e$  and  $f$  represents the 50  $\Omega$  input connector, the link line between nodes  $f$  and  $g$  represents the bond-wire inductance  $L_p$ , and the link line between nodes  $g$  and  $h$  represents the space-charge capacitance  $C_{sc}$ . The remaining reactive components  $C_p$  and  $C_s$ , are represented by transmission-line stubs. From the work of Johns and O'Brien [16], the impedances of the transmission lines are related to the component values and the iteration timestep  $\Delta T$  by:

$$Z_{C_p} = \Delta T / 2C_p \quad (1)$$

$$Z_{L_p} = L_p / \Delta T \quad (2)$$

$$Z_{C_s} = \Delta T / 2C_s \quad (3)$$

$$Z_{C_{sc}} = \Delta T / C_{sc} \quad (4)$$

The active region is represented by a Thevenin equivalent of a diode junction. The junction voltage,  $V_d$  and the junction impedance  $R_d$  are calculated from the average carrier density  $N$  at the junction for each iteration. This allows calculation of the current into the junction  $I_d$  from which a new carrier density can be calculated using a carrier density rate equation.

The junction voltage is calculated using

$$V_d = 0.05 \ln \left( \frac{N}{N_i} \right) \quad (5)$$

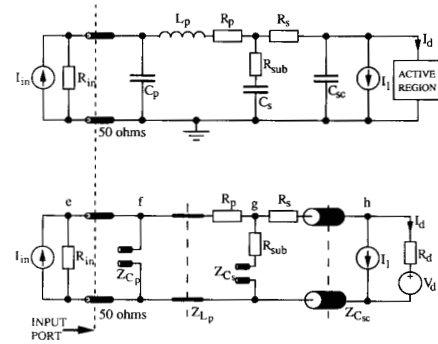


Fig. 3. Tucker's lumped component representation of the laser chip and package parasitics together with the equivalent transmission line representation.

TABLE I  
TRANSIENT RESPONSE TEST PARAMETERS

Symbol	Parameter Name	Value	Unit
$\lambda$	Wavelength	1.55	$\mu\text{m}$
$V$	Active region volume	60.0	$\mu\text{m}^3$
$a$	Gain cross section	$4.267 \times 10^{-16}$	$\text{cm}^2$
$N_0$	Transparency carrier density	$1.0 \times 10^{18}$	$\text{cm}^{-3}$
$N_i$	Intrinsic carrier density	$1.363 \times 10^{10}$	$\text{cm}^{-3}$
$\Gamma$	Waveguide confinement factor	0.3	
$\epsilon$	Gain compression factor	$6.7 \times 10^{-17}$	$\text{cm}^3$
$\bar{n}_e$	Group index of waveguide	4.0	
$\tau_r$	Carrier lifetime	3.0	ns
$\tau_p$	Photon lifetime	1.0	ps
$\beta$	Spontaneous coupling per laser chip mode	$2.0 \times 10^{-4}$	
$R_m$	Generator resistance	50.0	$\Omega$
$R_p$	Bond wire resistance	1.0	$\Omega$
$R_{sub}$	Chip substrate resistance	1.5	$\Omega$
$R_s$	Chip series resistance	5.5	$\Omega$
$C_p$	Bond wire capacitance	0.23	pF
$C_s$	Shunt parasitic capacitance	8.0	pF
$C_{sc}$	Space-charge capacitance	2.0	pF
$L_p$	Bond wire inductance	0.63	nH
$I_l$	Leakage current	0.0	mA
$\Delta T$	Model timestep	0.5	ps

The junction impedance is calculated using

$$R_d = \frac{0.05 \Delta T}{qVN} \quad (6)$$

where  $N_i$  is the intrinsic carrier density of the junction material,  $q$  is the electronic charge, and  $V$  is the volume of the active region.

The nodal voltages for a particular iteration are calculated using Thevenin equivalents of the transmission lines and the input source. The reflected waves, back into the lines, are then calculated using the fact that the sum of the incident and reflected waves equals the voltage at the end of the transmission line. The calculation of reflected waves from incident waves is known as *scattering* and may be represented by a scattering matrix. The incident waves at the next iteration are calculated from the reflected waves: waves into stubs are returned to the same scattering node; waves into link lines travel to adjacent

nodes. Calculation of the new incident waves from reflected waves is known as *connecting*. The network is solved by repeated application of the scatter-connect algorithm.

The junction current for a step-increase in input current was tested using timesteps of 0.1, 1, and 10 ps. No significant difference between the simulations was seen except for a small delay in the junction current rise when a 10 ps timestep was used. This can be explained by the delays of the link transmission lines. Because the timestep in the rest of the laser model is related to the propagation time across a section of the laser cavity, usually less than 1 ps, the model of the chip-and-package parasitics should be accurate for most situations [11]. Note that the transmission line representing the input connector is only one iteration timestep long and thus has a negligible effect on the simulations. Multiple-section lines could be used to gain a greater propagation delay through this connector.

### B. Nonlinear Gain

Tucker and Pope [17] and others, have demonstrated the importance of a nonlinear gain in damping the transient response of lasers. Until now, the transmission-line laser model has not accounted for nonlinear gain. To allow comparison results from a laser-transient response, the new model includes an empirical nonlinear gain term. Only the modifications to the TLLM [11] are described here.

The photon gain across a model section  $\exp(\gamma)$  is reduced by nonlinear gain. Here,  $\gamma$  is a gain constant, related to the carrier density  $N$  and the average photon density within the active region of the same section  $S_{\text{ave}}$  by

$$\gamma = [(N - N_0) a\Gamma (1 - \Gamma S_{\text{ave}}\epsilon) - \alpha_{\text{sc}}] \Delta L \quad (7)$$

where  $N$  is the average carrier density within a model section,  $N_0$  is the transparency carrier density,  $a$  is the gain cross section,  $\Gamma$  is the confinement factor of the optical guide,  $\alpha_{\text{sc}}$  is the cavity attenuation factor,  $\Delta L$  is the length of the section, and  $\epsilon$  is the gain-compression factor [14]. Note that the photon density is defined assuming all the photons travel within the active region so that the confinement factor  $\Gamma$  must be included in the nonlinear gain term.

The average photon density within a model section,  $S_{\text{ave}}$  can be related to the incident fields, assuming a constant carrier density within the section, by

$$S_{\text{ave}} = \bar{n}_e (|A^i|^2 + |B^i|^2) \cdot \frac{\exp \gamma' - 1}{\gamma' Z_p h f c m^2} \quad (8)$$

where  $\bar{n}_e$  is the group velocity in the active region,  $A$  and  $B$  are the forward- and backward-traveling optical fields incident on the section, defined below,  $Z_p$  is the cavity wave impedance [11],  $hf$  is the energy of a photon,  $c$  is the velocity of light,  $m$  is a unity constant with units of metres, and  $\gamma'$  is the gain constant for the previous iteration. This equation reduces, to (24), in [11] when  $\gamma \ll 1$ .

Earlier TLLM's assumed that the gain across a model section was small, allowing the stimulated emission rate to be calculated from the photon density at the input of a model section. To improve model accuracy for small numbers of sections in the new model, the stimulated recombination rate in a section  $R_{\text{stim}}$  is calculated using

$$R_{\text{stim}} = S_{\text{ave}} \cdot ac\Gamma(N - N_0)/\bar{n}_e. \quad (9)$$

### III. APPLICATIONS OF THE MODEL

Three examples have been chosen to demonstrate the flexibility of the model and the use of the bidirectional interfaces. Schematics of the three numerical experiments are shown in Fig. 4 and the experiments are detailed as follows.

#### A. Transient Response of a Semiconductor Laser

This example shows the importance of including the nonlinear gain, chip, and package parasitics [Fig. 4(a)] when simulating transient responses of lasers and tests the model against the equivalent-circuit model in [14]. Adding the parasitics to the model requires that the chip model have a bidirectional port: this example demonstrates the bidirectional electrical port. The parameters used were for a ridge-waveguide laser and are given in Table I. As the equivalent circuit model in [14] assumed a single longitudinal mode, the new model was operated in the single-mode regime. Single-mode operation requires that a single model section be used to represent the laser chip, otherwise the spontaneous noise bandwidth would be too large [11]. Using one section gives a large photon density variation across the section ( $\gamma > 1$ ) justifying the use of (9).

The model (neglecting chip-and-package parasitics) was tested by simulating a laser transient against 1) a simple rate-equation based model and 2) Tucker and Kaminow's equivalent circuit of the rate equations [14]. As all TLLM's use a random noise source to model spontaneous emission [13], the spontaneous emission coupling factor  $\beta$  was set to  $1 \times 10^{-6}$  to minimize noise on the intensity waveform in these simulations. Excellent agreement was obtained between all the models when timesteps below 1 ps were used. This test showed that the gain saturation term is capable of damping a laser's transient response when the spontaneous emission coupling is very low. This test also showed that the new model is accurate with only a single model section. As the computation time is proportional to the square of the number of sections [11], this is obviously an important conclusion.

In real devices, noise-induced variations between subsequent transients cause broadening of sampling oscilloscope traces. When the spontaneous emission coupling is set to a realistic value, the model also produces noise induced variations in the transients. We simulated the effect of a sampling oscilloscope by overlaying the sample points from 100 individual simulations, as shown in Fig. 5. Two bias levels of 98% and 111% of threshold were used to allow comparison with Tucker and Kaminow's Fig. 13(a)

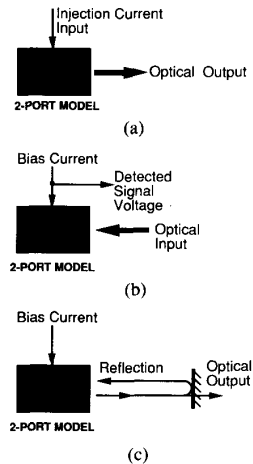


Fig. 4. Schematics of three examples of the use of the two-port model. (a) Laser transient response, (b) laser as a detector, and (c) coherence collapse in a laser with moderate reflectivity from an external reflector.

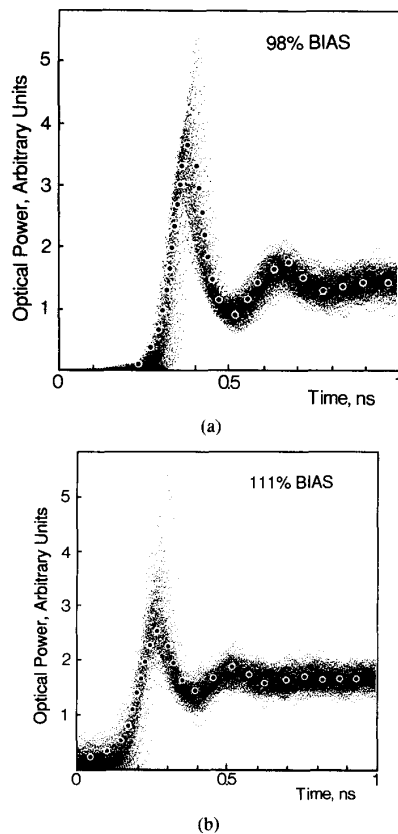


Fig. 5. Laser transient response modeled using the transmission-line model (broad trace) and measured (dots). (a) 98% bias and (b) 103% bias. The measured result is from Tucker and Kaminow [14].

and (b) [14]. The laser was driven with pulses 40 mA above the bias level with a 100 ps risetime. Note that this current is the net current flowing into the laser package and not the current flowing into the package and the 50  $\Omega$  source impedance. Comparison between (a) and (b) shows

that the laser is better damped when turning on from a higher bias level. Also plotted as dots in Fig. 5(a) and (b) are the experimental measurements in Tucker and Kaminow's Fig. 13(a) and (b), respectively. The dots lie toward the center of the simulated trace, indicating that the model is in good agreement with the experiment.

The broad traces at the leading edges of the transients in Fig. 5 indicate turn-on timing jitter. Turn-on timing jitter was investigated numerically by Miller [18] and was shown to be a result of the intensity noise before the laser turn-on. The traces also show a large scatter in points around the first peak of the transient. This scatter arises because the carrier density before the first optical pulse is dependent on when the laser turns on: a slow-to-turn-on laser will build up a higher carrier density that will produce an initial pulse with more energy. Fig. 5 also shows a large intensity noise once the transient has settled. Such a noise was also simulated by Miller and Marcuse [19] and is discussed further in Section III-C. Spano *et al.* have measured the rms-timing jitter of a single-mode laser and have developed a comprehensive theory that gives good agreement with measurements [20]. The simulated pulse in Fig. 5(a) shows a similar jitter to their sampling oscilloscope measurement (Fig. 2, [20]). They calculate an rms jitter of around 10 ps for a laser with a similar threshold and output power. Inspection of Fig. 5(a) shows that the TLLM produces an rms jitter close to 10 ps.

#### B. Use of a Laser as an Optical Detector

Gustavsson *et al.* [21] have used laser amplifiers as optical detectors with inbuilt gain with the optical signal coupled into one antireflection-coated facet of the laser [Fig. 4(b)]. The output signal appears across the junction of the laser when it is biased with a constant current to produce population inversion. A voltage change up to 250  $\mu$ V for an optical power change of 1  $\mu$ W has been reported [21]. Because the laser has a low impedance (a few ohms) when forward biased, the output of this detector can drive a low impedance load. The new model is able to simulate laser detectors because of its bidirectional optical and electrical interfaces; the facet becomes an optical input and the electrical contact is the signal output. The frequency response, saturation characteristic, and effect of contact position is discussed.

*Laser Amplifier Detector Frequency Response:* The parameters of the laser amplifier detector are given in Table II. The model included chip-and-package parasitics as detailed in Table I. An eight-section model was used, with eight carrier rate equations, to allow inhomogeneities in the carrier density. Because the gain of laser amplifiers along their length is high, 15.6 dB in this case, the carrier density is unevenly saturated over the amplifier length, leading to large inhomogeneities [5].

The optical wave into the amplifier was on an amplifier resonance and was modulated with a square wave to 100% modulation depth. The peak input power is defined as that just outside the amplifier input facet and was  $-20$  dBm (10  $\mu$ W). The peak-to-peak contact voltage response to the optical input is plotted against modulation frequency

TABLE II  
AMPLIFIER DETECTOR TEST PARAMETERS<sup>a</sup>

Symbol	Parameter Name	Value	Unit
$L$	Laser chip length	300.0	$\mu\text{m}$
$w$	Active region width	2.0	$\mu\text{m}$
$d$	Active region depth	0.15	$\mu\text{m}$
$a$	Gain cross section	$2.5 \times 10^{-16}$	$\text{cm}^2$
$\alpha_{\text{sc}}$	Waveguide attenuation factor	30.0	$\text{cm}^{-3}$
$R$	Facet reflectivities	0.01	%
$A$	Monomolecular recomb. coef.	$1.0 \times 10^8$	$\text{s}^{-1}$
$B$	Bimolecular recomb. coef.	$8.6 \times 10^{-11}$	$\text{cm}^3 \cdot \text{s}^{-1}$
$C$	Auger recomb. coef.	$4.0 \times 10^{-29}$	$\text{cm}^6 \cdot \text{s}^{-1}$
$\beta$	Spontaneous coupling per laser chip mode	0.0	
$I_{\text{bias}}$	Amplifier bias current	55.0	mA

<sup>a</sup>All other parameters are as Table I.

in Fig. 6. The  $-3$  dB (electrical) point was 700 MHz. The response at low frequencies was around  $31 \mu\text{V}/\mu\text{W}$  input. The upper-frequency is proportional to the inverse of the carrier recovery time, which is dependent on the carrier density [22]. It is, therefore, advantageous to maximize the carrier density by high bias to minimize the carrier recovery time.

**Laser Amplifier Detector Saturation Characteristic:** All semiconductor laser amplifiers suffer from reduced gain when the input signal is large [23]. Fig. 7 shows the saturation characteristic for our device at a modulation frequency of 125 MHz. The model was run for several cycles to allow the carrier density to stabilize and give a CW characteristic. At input powers below  $100 \mu\text{W}$  the device operated linearly. The output was reduced by 3 dB (electrical) from its unsaturated value at an input power of about  $400 \mu\text{W}$ . At input powers above  $10 \text{ mW}$  the output voltage reduced as the input voltage was increased. This behavior is a result of the carrier density being reduced to a level near the transparency carrier density at high input powers. Because the gain is reduced, the change in carrier density per unit change in input power is reduced. Thus, the contact voltage modulation is reduced.

**Laser Amplifier Detector Contact Position Optimization:** If the amplifier has a single contact, the contact voltage modulation will be an average of the junction voltage modulation along the amplifier length. However, if the contact is split into sections, then each contact section will respond to the junction voltage beneath it. Because of the longitudinal gain, contacts away from the input facet of the amplifier will detect an increased signal level. Note that all contacts should have an appropriate proportion of the bias current applied to them.

The new model is already divided into sections, each with a separate carrier density model. This allows for investigation of the multiple-contact amplifier. Fig. 8 shows the contact voltage modulation for an input power of  $10 \mu\text{W}$  at 125 MHz. The peak-peak contact voltage increased exponentially with contact position as expected if the gain is constant along the laser chip (i.e., no gain saturation) [23]. This result indicates that the optimum arrangement is a split contact with a long section at the in-

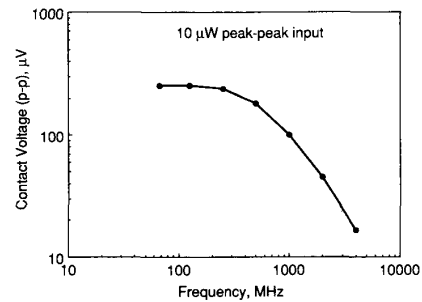


Fig. 6. Frequency response of the laser detector ( $10 \mu\text{W}$  peak input power).

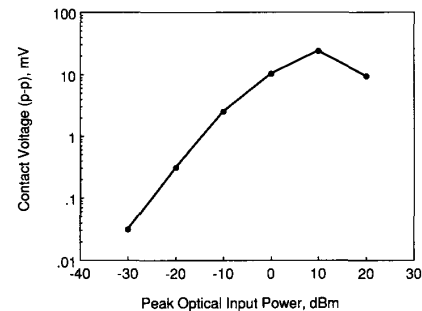


Fig. 7. Electrical output (peak-peak) versus optical peak power of the laser detector at 125 MHz.

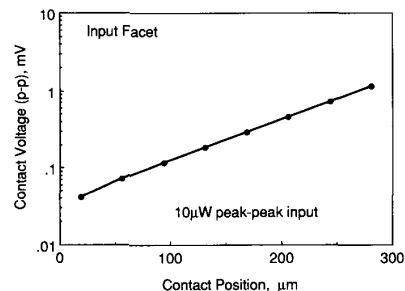


Fig. 8. Output voltage versus contact position for the laser detector for  $10 \mu\text{W}$  input power at 125 MHz.

put end of the amplifier and a short section at the far end of the amplifier. Both sections would provide bias to the amplifier and the short section would also provide a signal output. Such an arrangement would provide 5.6 dB improvement in signal level over the signal-contact amplifier in this case. However, if the signal contact was too small the impedance of the detector would rise, giving increased noise.

### C. Coherence Collapse in a Laser with Weak Optical Feedback

Because the model includes a bidirectional optical port it can be used to assess the effects of optical feedback into the laser [Fig. 4(c)]. One widely reported effect of medium levels ( $-40$  dB to  $-10$  dB) of optical feedback is coherence collapse; coherence collapse refers to a large broadening of the laser's linewidth to tens of gigahertz

TABLE III  
COHERENCE COLLAPSE TEST PARAMETERS<sup>a</sup>

Symbol	Parameter Name	Value	Unit
$\alpha$	Linewidth enhancement factor	5.6	
$R$	Facet reflectivities	30.0	%
$\beta$	Spontaneous coupling per laser chip mode	$1.0 \times 10^{-4}$	
$L_e$	External cavity length	12.0	cm
$I_{\text{bias}}$	Laser bias current	20.0	mA

<sup>a</sup>All other parameters are as Table II.

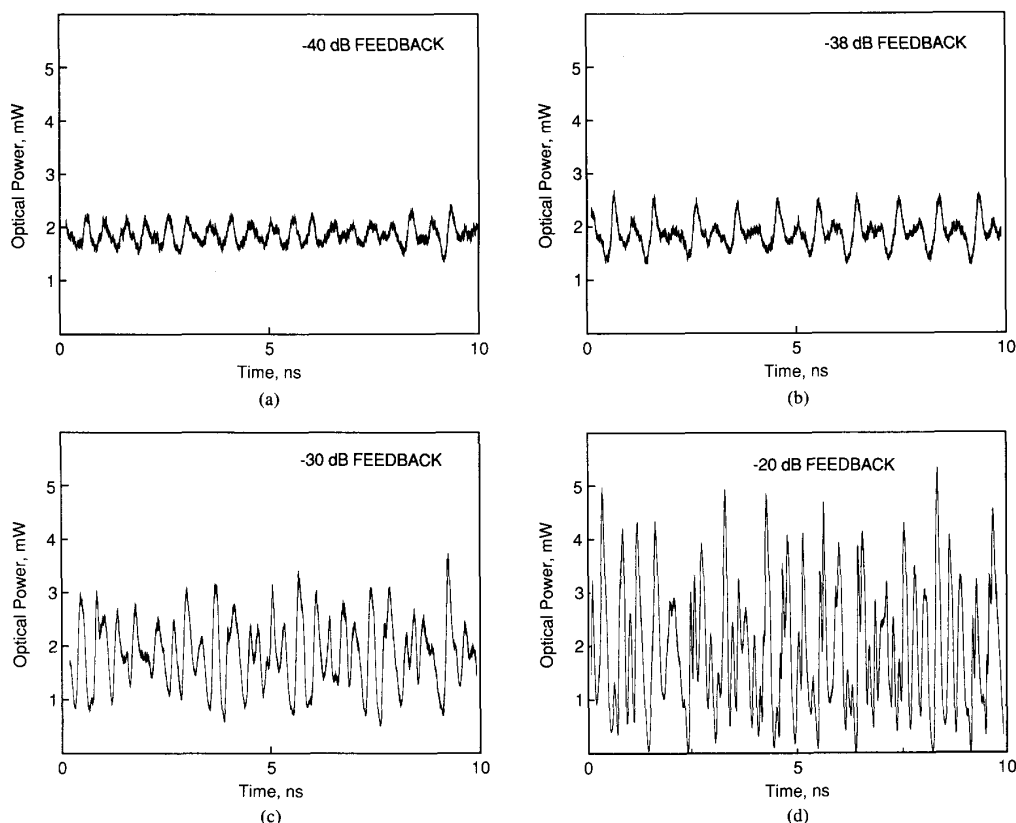


Fig. 9. Intensity waveform of the laser with external reflectivity. The feedback levels were (a) -40 dB, (b) -38 dB, (c) -30 dB, and (d) -20 dB.

[24]–[28]. Accompanying the massive broadening is an increase in intensity noise [28]–[29]. Coherence collapse is detrimental to the operation of both FM- and AM-modulated optical communication systems.

Models of coherence collapse have been presented by many authors [24], [30]–[34]. This example shows that the new model can also predict coherence collapse by feeding back optical field samples into the bidirectional optical port after an appropriate delay [11]. Unlike some analytical models, the new model neither assumes coherent feedback [31], [32] or incoherent feedback [24], [33]. Such assumptions are not required because the time-domain bidirectional optical interface describes the optical wave over a large optical bandwidth because optical field is used as a variable [35]. Thus, both narrow-linewidth and coherence-collapsed feedback are correctly treated.

Also, because the interface is in terms of optical field, the phase of the feedback is included.

The test parameters for this example are given in Table III. The model included carrier dependent refractive index as this is essential to the coherence collapse process [29]. Details of the refractive index model are given in [11]. Spontaneous emission noise was represented by random noise generators in every section. Gain wavelength dependence was included in the model to ensure single-mode operation. Chip-and-package parasitics were not included. The laser was biased to give a mean output of 1.9 mW.

Fig. 9 shows the power waveforms, obtained by squaring the optical field and averaging over 10 iterations, for four levels of optical feedback. At -40 dB feedback [Fig. 9(a)] the laser showed a strong resonance at 2 GHz, the

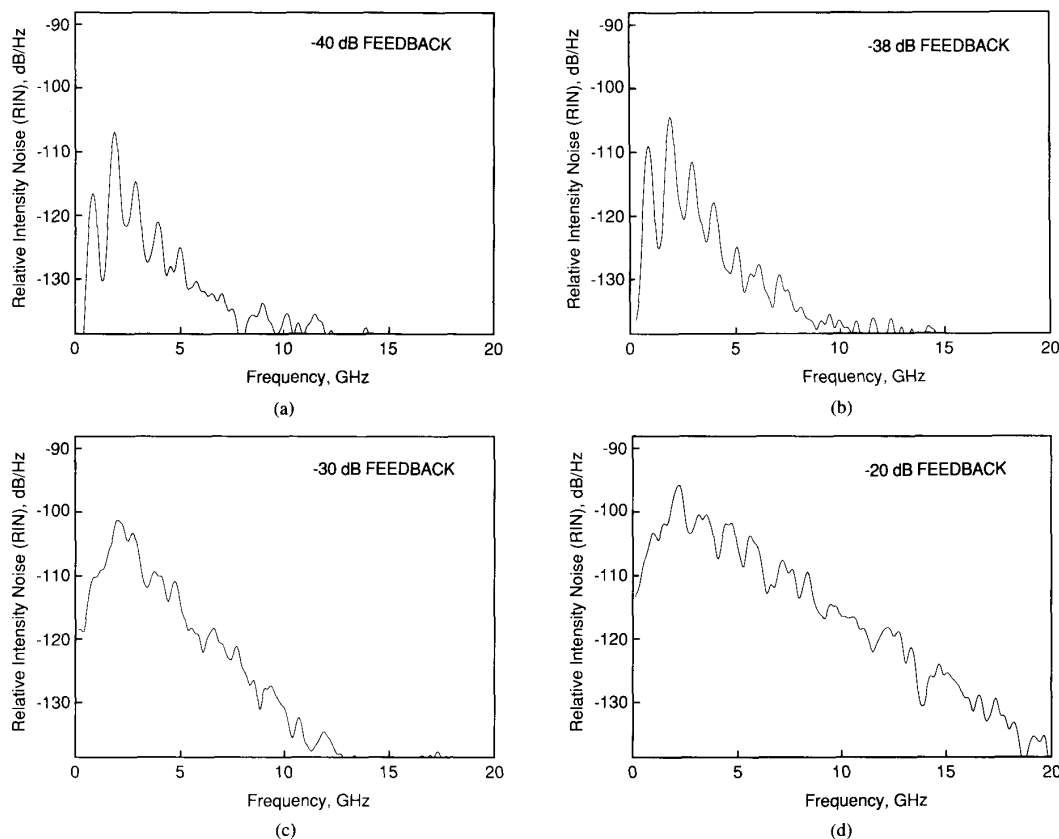


Fig. 10. Intensity noise spectrum of the laser with external reflectivity. The feedback levels were (a)  $-40$  dB, (b)  $-38$  dB, (c)  $-30$  dB, and (d)  $-20$  dB.

external cavity resonance frequency. At  $-38$  dB feedback [Fig. 9(b)] the period of the resonance doubled and the resonance became stronger. At  $-30$  dB feedback [Fig. 9(c)] the power waveform appears to be chaotic and aperiodic and has a modulation depth of around 50%. At  $-20$  dB feedback [Fig. 9(d)] the modulation depth of the chaotic behavior was almost 100%. These power waveforms are similar to those obtained by Dente *et al.* using rate equations and assuming coherent feedback [26]. However, the depth of modulation in the coherence collapsed state [Fig. 9(c)] is much larger here. This difference may be because this model feeds back incoherent light when in an incoherent (collapsed) state. These waveforms suggest that period doubling is the route to chaos, as proposed by Mukai and Otsuka [34].

Fourier transformation of the data in Fig. 9, followed by convolution with a Gaussian bell with  $\sigma = 120$  MHz to remove noise, gives the intensity spectra shown in Fig. 10. At  $-40$  dB feedback [Fig. 10(a)] the intensity spectrum had distinct peaks at harmonics of 1 GHz, half the external cavity resonance frequency. The 1 GHz peak was  $-10$  dB below the 2 GHz peak. At  $-38$  dB feedback [Fig. 10(b)], the resonance peaks were still visible. However, the 1 GHz component was increased in amplitude to 4 dB below the 2 GHz peak. This increase is consistent with the period doubling seen in Fig. 9(b) [34]. At  $-30$  dB

feedback [Fig. 10(c)] the intensity noise increased over the entire frequency range. The intensity spectrum peaked near to the electron-photon populations' resonance frequency (2.8 GHz). At  $-20$  dB feedback [Fig. 10(d)] the intensity noise was large over the entire bandwidth. Comparison with the noise spectrum of a laser without feedback indicates that the noise increased by at least 20 dB over the entire frequency range. The dramatic increase in noise at feedback levels above  $-40$  dB is consistent with the numerical results of Schunk and Petermann [29]. The spectra on RIN levels are similar to those measured experimentally over the range 0–2 GHz by Woodward, Koch, and Koren [28].

Fig. 11 shows the optical spectra obtained by Fourier transformation of the optical field output of the model for the levels of optical feedback with in Figs. 9 and 10. At  $-40$  dB feedback [Fig. 11(a)] the optical spectrum was a single narrow line with sidebands spaced at the external cavity resonance frequency. At  $-38$  dB feedback [Fig. 11(b)] the number of peaks increased and the spectrum became highly asymmetrical. This asymmetry was explained theoretically by Cohen and Lenstra as being the result of amplitude fluctuations [33]. Goldberg *et al.* have also measured large asymmetries in the optical spectrum [27]. At  $-30$  dB feedback [Fig. 11(c)] the spectrum broke up into many peaks with no apparent relation between the

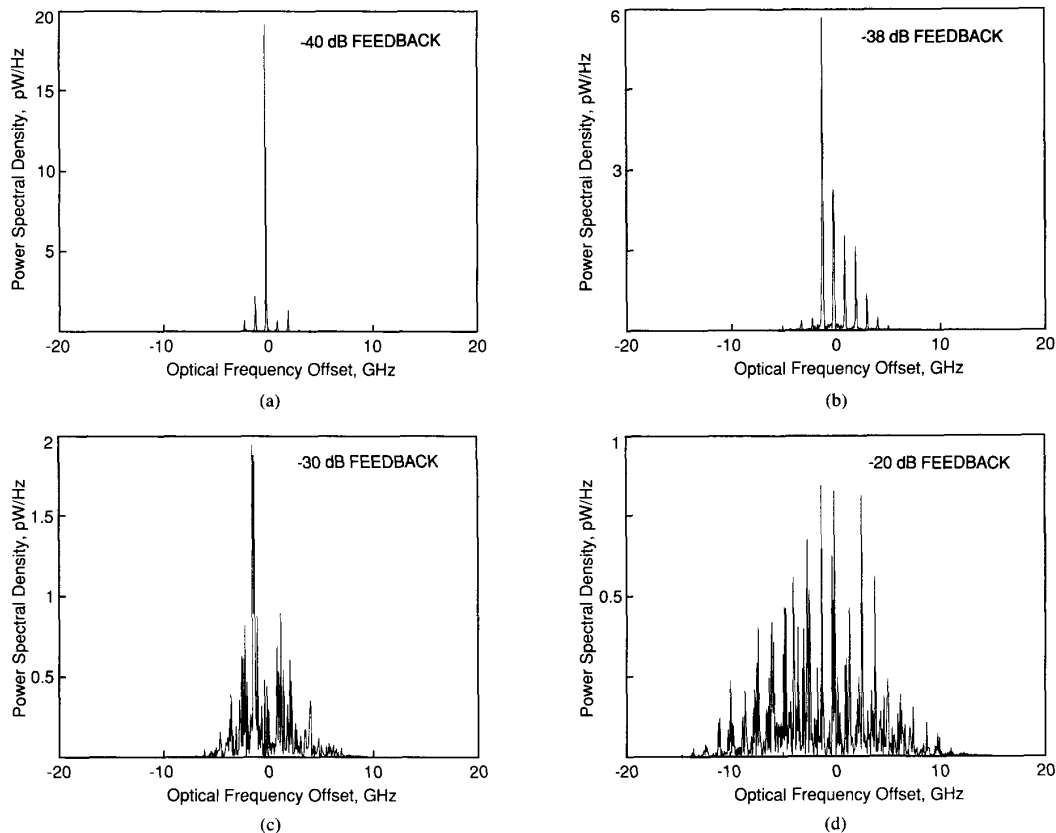


Fig. 11. Optical spectrum of the laser with external reflectivity. The feedback levels were (a)  $-40$  dB, (b)  $-38$  dB, (c)  $-30$  dB, and (d)  $-20$  dB.

peaks' frequencies. The spectral width was over 10 GHz, indicating coherence collapse. At  $-20$  dB feedback [Fig. 11(d)] the spectrum broadened to over 25 GHz. The spectral peaks fell into groups spaced at about 1 GHz, consistent with period doubling [34]. The spectral behavior shown in Fig. 11 is in agreement with experimental measurements by Tkach and Chraplyvy for a DFB laser [25], by Woodward *et al.* for DBR lasers [28] and for Fabry-Perot lasers by Dente *et al.* [26].

The feedback level at which coherence collapse occurs is believed to be independent of cavity length [28] and is defined as the level at which the sidebands first appear in the optical spectrum [25] or the level at which the optical spectrum collapses into many lines [29]. Sidebands first appear at a feedback level between  $-42$  and  $-40$  dB in our laser and the spectrum collapses into many lines between  $-35$  and  $-30$  dB. These results are in broad agreement with [25], [27], [28].

Deterministic chaos has been cited as the cause of coherence collapse [26], [34]. The simulations here included noise terms, so the simulated coherence collapse could have been caused by this noise. To test the effect of the noise, the noise generators were turned off after the initial laser transient. A similar intensity waveform was obtained for  $-20$  dB feedback but with slightly higher

peaks. The noise is thought to damp these peaks in a similar manner to noise-damping laser turn-on transients. Coherence collapse in the absence of noise suggests a chaotic mechanism [26].

#### IV. CONCLUSION

This paper has introduced a new model for semiconductor lasers, based on a combination of two earlier models. The new model includes bidirectional electrical and optical ports making it extremely flexible. The ports allow interconnection with other models, such as for drive circuits and for external optical components.

Three examples of the use of the model were given:

1) A laser transient response was modeled and excellent agreement was obtained with previous results. The transient response also showed large timing jitters and intensity noise.

2) A laser used as a detector was assessed. Its frequency response was flat until 700 MHz and then rolled off at 20 dB/decade. The laser detector had a linear transfer characteristic up to 100  $\mu$ W input power (peak-peak). Dividing the contact into sections and then using the section furthest from the optical input was found to improve the output signal level by 5.6 dB.

TABLE IV  
APPLICATIONS OF THE TWO-PORT MODEL

Application	Tested On	References
Laser transient response	FP, EC, DFB, ML	[11]
Laser turn-on jitter	FP	This paper
Laser spectrum	FP, EC, DFB, ML	[11]
Laser chirp	FP, EC, DFB, ML	[11,36]
Laser intensity noise	FP, ML	This paper, [11]
Laser RIN spectra	FP, ML	This paper
Coherence collapse	FP	This paper
Laser as a receiver	FP, TWLA	This paper

Key: FP = Fabry-Perot laser; DFB = distributed feedback laser; EC = external-cavity laser; ML = mode-locked laser.

3) The behavior of a laser with moderate amounts of optical feedback was studied. Coherence collapse, leading to intensity fluctuations, spectral broadening, and massive increases in linewidth, was observed at feedback levels above  $-40$  dB. The observations were in good agreement with other workers' experimental results.

Because the model was developed from the TLLM, which has already been applied to a variety of laser structures other than simple Fabry-Perot resonators studied here, the model should be applicable to a variety of laser structures. Table IV summarizes the applicability of the model and includes appropriate references for the types of device that the TLLM has been applied to. In theory, the applications could be applied to all types of lasers.

This paper has already demonstrated the flexibility of the model and its ability to produce realistic results for a variety of experimental situations without modification. The use of a single model for many applications has the advantage, over separate models for each case, in that errors in programming are quickly spotted. Also, a model not tailored to a specific application is more likely to predict unusual behaviors of devices, such as the period doubling route to chaos. Future work will generate new applications of the model. Some examples are RIN of complex laser structures such as DBR's, stability of lasers with feedback, and application of the model to optical systems modeling. The development of a CAD system for photonic devices and systems, based on this model, is already underway at Melbourne University.

#### ACKNOWLEDGMENT

The author wishes to thank Prof. R. S. Tucker of Melbourne University for discussions on equivalent circuit models and Dr. K. Delong of NTT, Tokyo, and Dr. M. Landman of BHP Research, Australia, for discussions on chaos.

#### REFERENCES

- [1] J. Buus, "Principles of semiconductor laser modelling," *IEE Proc. J., Optoelectron.*, vol. 132, pp. 42-51, 1985.
- [2] P. M. Boers, M. T. Vlaardingbroek, and M. Danielsen "Dynamic

- behavior of semiconductor lasers," *Electron. Lett.*, vol. 11, pp. 206-208, 1975.
- [3] H. Hillbrand and P. Russer, "Large signal PCM behavior of injection lasers with coherent radiation into one of their oscillating modes," *Electron. Lett.*, vol. 11, pp. 372-374, 1975.
- [4] M. Osinski and M. J. Adams, "Transient time-averaged spectra of rapidly-modulated semiconductor lasers," *IEE Proc. J. Optoelectron.*, vol. 132, pp. 34-37, 1985.
- [5] A. J. Lowery, "Modelling ultra-short pulses (less than the cavity transit time) in semiconductor laser amplifiers," *Int. J. Optoelectron.*, vol. 3, pp. 497-508, 1988.
- [6] M. S. Demokan, "A model of a diode laser actively mode-locked by gain modulation," *Int. J. Electron.*, vol. 60, pp. 67-80, 1986.
- [7] L. A. Coldren and T. L. Koch, "Analysis and design of coupled-cavity lasers: Part 2: Transient analysis," *IEEE J. Quantum Electron.*, vol. 20, pp. 671-681, 1984.
- [8] J. E. Whiteaway, G. H. B. Thompson, A. J. Collar, and C. J. Armistead, "The design and assessment of  $\lambda/4$  phase-shifted DFB structures," *IEEE J. Quantum Electron.*, vol. 25, pp. 1261-1279, 1989.
- [9] R. S. Tucker, "High-speed modulation of semiconductor lasers," *J. Lightwave Technol.*, vol. LT-3, pp. 1180-1192, 1985.
- [10] G. Bjork and O. Nilsson, "A new exact and efficient numerical matrix theory of complicated laser structures: Properties of asymmetric phase-shifted DFB lasers," *J. Lightwave Technol.*, vol. LT-5, pp. 140-146, 1987.
- [11] A. J. Lowery, "Transmission-line modelling of semiconductor lasers: The transmission-line laser model," *Int. J. Numer. Model.*, vol. 2, pp. 249-265, 1990.
- [12] — "A new dynamic model for multimode chirp in DFB semiconductor lasers," *IEE Proc. J. Optoelectron.*, vol. 137, pp. 293-300, 1990.
- [13] — "Amplified spontaneous emission in semiconductor laser amplifiers: The validity of the transmission-line laser model," *IEE Proc. J. Optoelectron.*, vol. 137, pp. 241-247, 1990.
- [14] R. S. Tucker and I. P. Kaminow, "High-frequency characteristics of directly modulated InGaAsP ridge waveguide and buried heterostructure lasers," *J. Lightwave Technol.*, vol. LT-2, pp. 385-393, 1984.
- [15] L. W. Nagel, "SPICE2: A computer program to stimulate semiconductor circuits," *Electron. Res. Lab.*, Univ. California, Berkeley, CA, Ref. ERL-M520, 1975.
- [16] P. B. Johns and M. O'Brien, "Use of the transmission-line modelling (TLM) method to solve non-linear lumped networks," *Radio and Electron. Eng.*, vol. 50, pp. 57-90, 1980.
- [17] R. S. Tucker and D. J. Pope, "Circuit modeling of the effect of diffusion on damping in a narrow-stripe semiconductor laser," *IEEE J. Quantum Electron.*, vol. QE-19, pp. 1179-1183, 1983.
- [18] S. E. Miller, "Turn-on jitter in nearly single-mode injection lasers," *IEEE J. Quantum Electron.*, vol. QE-22, pp. 16-19, 1986.
- [19] S. E. Miller and D. Marcuse, "On fluctuations and transients in injection lasers," *IEEE J. Quantum Electron.*, vol. QE-20, pp. 1032-1044, 1984.
- [20] P. Spano, A. D'Ottavi, A. Mecozzi, B. Daino, and S. Piazzolla, "Experimental measurements and theory of first passage time in pulse-modulated semiconductor lasers," *IEEE J. Quantum Electron.*, vol. 25, pp. 1440-1449, 1989.
- [21] M. Gustavsson, A. Karlsson, and L. Thylen, "Traveling wave semiconductor laser amplifier detector," *J. Lightwave Technol.*, vol. 8, pp. 610-617, 1990.
- [22] G. Eisenstein, R. S. Tucker, J. M. Weisenfeld, P. B. Hansen, G. Raybon, B. C. Johnson, T. J. Bridges, F. G. Storz, and C. A. Burrus, "Gain recovery time of travelling-wave semiconductor laser amplifiers," *Appl. Phys. Lett.*, vol. 54, pp. 454-456, 1989.
- [23] J. C. Simon, "Semiconductor laser amplifier for single-mode optical fibre communications," *J. Opt. Commun.*, vol. 4, pp. 51-62, 1983.
- [24] D. Lenstra, B. H. Verbeek, and A. J. den Boef, "Coherence collapse in single-mode semiconductor lasers due to optical feedback," *IEEE J. Quantum Electron.*, vol. QE-21, pp. 674-679, 1985.
- [25] R. W. Tkach and A. R. Chraplyvy, "Regimes of feedback effects in  $1.5 \mu\text{m}$  distributed feedback lasers," *J. Lightwave Technol.*, vol. LT-4, pp. 1655-1661, 1986.
- [26] G. C. Dente, P. S. Durkin, K. A. Wilson, and C. A. Moeller, "Chaos in the coherence collapse of semiconductor lasers," *IEEE J. Quantum Electron.*, vol. 24, pp. 2441-2447, 1988.
- [27] L. Goldberg, H. F. Taylor, A. Dandridge, J. F. Weller, and R. O. Miles, "Spectral characteristics of semiconductor lasers with optical feedback," *IEEE J. Quantum Electron.*, vol. QE-18, pp. 555-563, 1982.

- [28] S. L. Woodward, T. L. Koch, and U. Koren, "The onset of coherence collapse in DBR lasers," *IEEE Photon. Technol. Lett.*, vol. 2, pp. 391-394, 1990.
- [29] N. Schunk and K. Petermann, "Numerical analysis of the feedback regimes for a single-mode semiconductor laser with external feedback," *IEEE J. Quantum Electron.*, vol. 24, pp. 1242-1247, 1988.
- [30] H. Olesen, J. H. Osmundsen, and B. Tromborg, "Nonlinear dynamics and spectral behavior for an external cavity laser," *IEEE J. Quantum Electron.*, vol. 22, pp. 762-773, 1986.
- [31] R. Lang and K. Kobayashi, "External optical feedback effects on semiconductor injection laser properties," *IEEE J. Quantum Electron.*, vol. 16, pp. 347-355, 1980.
- [32] C. H. Henry and R. F. Kazarinov, "Instability of semiconductor lasers due to optical feedback from distant reflectors," *IEEE J. Quantum Electron.*, vol. 22, pp. 294-301, 1986.
- [33] J. S. Cohen and D. Lenstra, "Spectral properties of the coherence collapsed state of a semiconductor laser with delayed optical feedback," *IEEE J. Quantum Electron.*, vol. QE-25, pp. 1143-1151, 1989.
- [34] T. Mukai and K. Otsuka, "New route to optical chaos: Successive subharmonic-oscillation cascade in a semiconductor laser coupled to an external cavity," *Phys. Rev. Lett.*, vol. 55, pp. 1711-1714, 1985.
- [35] R. Lang and K. Kobayashi, "External optical feedback effects on semiconductor laser properties," *IEEE J. Quantum Electron.*, vol. QE-16, pp. 347-355, 1980.
- [36] A. J. Lowery, "Time resolved chirp in mode-locked semiconductor lasers," *Electron. Lett.*, vol. 26, pp. 939-940, 1990.



**Arthur James Lowery** was born in Yorkshire, England, on October 17, 1961. He received the First Class Honours degree in applied physics from Durham University, England, in 1983, and the Ph.D. degree in 1988 from the University of Nottingham.

He then worked as a Systems Engineer at Marconi Radar Systems. In 1984 he was appointed a University Lecturer at the University of Nottingham. In 1990 he became a Senior University Lecturer in the newly formed Photonics Research

Laboratory, University of Melbourne, Australia. He has published more than 40 research papers in the fields of photonics and numerical modeling. His research interests include photonic CAD, mode-locked lasers, laser amplifiers, photonic switching, optical metrology, fiber video distribution, transmission-line modeling, and laser design.

Dr. Lowery is a Chartered Engineer and a member of the Institution of Electrical Engineers.